

WELD RESIDUAL STRESSES MODELLING. APPLICATION TO A NUCLEAR POWER PLANT WELDED JOINT.

Alejandro Cosimo^{a,c}, Alberto Cardona^a, Pablo Novara^a and Nestor Calvo^b

^a*Centro de Investigación de Métodos Computacionales (CIMEC), Universidad Nacional del Litoral-CONICET, Predio CONICET ruta 168, S3000GLN Santa Fe, Argentina*

^b*Universidad Nacional del Litoral, Santa Fe, Argentina*

^c*Becario de la Autoridad Regulatoria Nuclear*

Keywords: Weld Residual Stresses; Welding simulation; Computational Welding Mechanics; Finite Elements; Stress Corrosion Cracking; SCC; WRS

Abstract.

Stress Corrosion Cracking (SCC) is a mechanism of failure associated to the growth of long circumferential cracks in welded pipes. Weld Residual Stresses (WRS) highly influence this mechanism of failure. Therefore, the knowledge of residual stresses becomes fundamental in order to predict the growth of cracks by SCC. In this work a weakly coupled thermo-mechanical model is used for modelling the welding process of a large nuclear power plant structure in order to predict WRS. Specifically, the simulation of the welding process of a nozzle weld that connects the reactor pressure vessel and the cold leg of a nuclear reactor facility is studied.

1 INTRODUCTION

Two mechanisms of failure can be identified in welded joints of nuclear power plant structures: failure by fatigue, and failure by Stress Corrosion Cracking (SCC). The worst case scenario is stated by the SCC, mechanism that is highly influenced by Weld Residual Stresses (WRS). The objective of this work is the prediction of WRS by simulating the whole welding process. Modelling of Post Weld Heat Treatment (PWHT) is left as future work.

In this work, the welding process of the nozzle weld that connects the Reactor Pressure Vessel (RPV) and the cold leg of a nuclear power plant is studied and modelled. In Figure 1 details of the nozzle to be modelled can be observed.

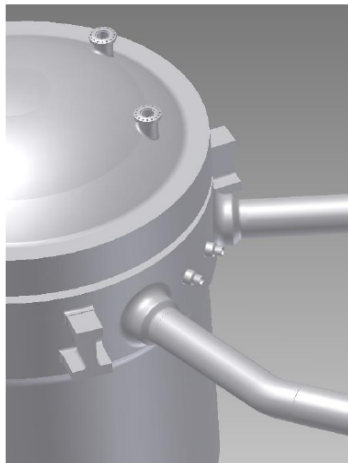


Figure 1: Detail of the nozzle weld that connects the reactor pressure vessel and the cold leg.

This work is organised as follows. First a description of the problem is given. Then in Section 3, details of the numerical model are provided. The thermal and mechanical properties of the involved materials are specified as part of Section 4. In Section 5 the obtained results are exposed and discussed. Finally, the conclusions are given.

2 PROBLEM DESCRIPTION

The problem consists in the simulation of the welding process of the nozzle weld that connects the RPV and the cold leg. Initially, a cladding layer of approximately 5mm is deposited in the interior of the pipe. Once the cladding deposition is finished, a thermal treatment is applied in order to remove the generated residual stresses. Therefore, it is considered that the cladding process does not contribute to residual stresses and at the beginning of the welding process the initial configuration is assumed to be a stress free configuration. Before the welding of the nozzle and the pipe is started a preheating stage takes place rising the temperature of the zone to be welded from ambient temperature to 160 °C. In order to model the preheating stage, an initial homogeneous temperature equal to 160 °C is taken for the whole domain.

In what follows details of the problem to be modelled are given. A longitudinal section of the involved pipes can be observed in Figure 2, where the inner diameter of the nozzle and the pipe is 750mm. Details of the geometry and the welding plan can be observed in Figure 3a. A macrograph specifying the material denomination of each of the components of the weld is shown in Figure 3b. Based on the dimensions characterising the problem, it must be noted that a three dimensional analysis would be very computationally intensive making this option

prohibitive and impractical. That is why a two dimensional axisymmetric analysis seems more reasonable for the current case. The error introduced is not high if it is considered that the longitudinal section under analysis is away from the starting and ending points of the welding process.

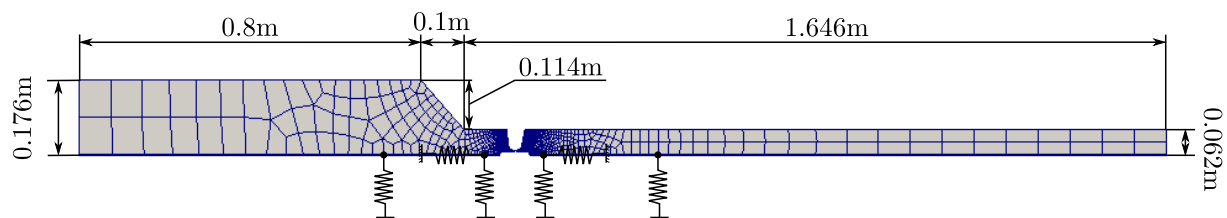
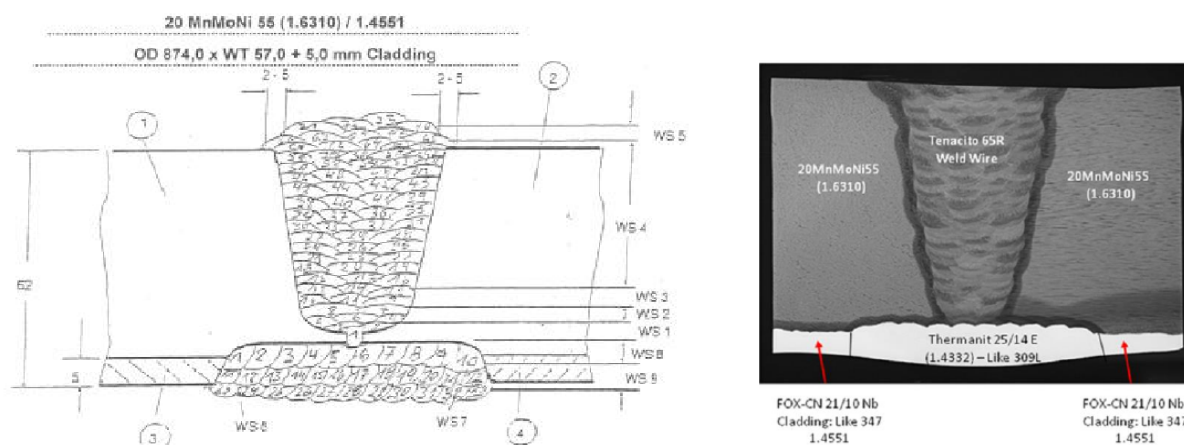


Figure 2: Longitudinal section of the involved pipes. Specification of the domain and mesh to be used in the two dimensional analysis of the problem.



(a) Graphical longitudinal section of the welding plan and expected final geometry. (b) Specification of the materials used in each region of the weld.

Figure 3: Details of the problem: welding plan and material denominations.

The boundary conditions of the thermal problem are given by Robin boundary conditions at the internal and external faces of the nozzle and the pipe, including the evolving boundary of the deposited weld beads. Both ends of the tube are modelled with adiabatic boundary conditions. In the mechanical problem, free traction boundary conditions are imposed everywhere, and the system is supported by means of the springs depicted in Figure 2. This is justified because in the real facilities, in order to deal with thermal deformations every structural component of the plant is elastically supported to the RPV by means of springs and bellows pipes. The springs used for the numerical analysis of the welding process, have a very low stiffness constant and are used to avoid singularities.

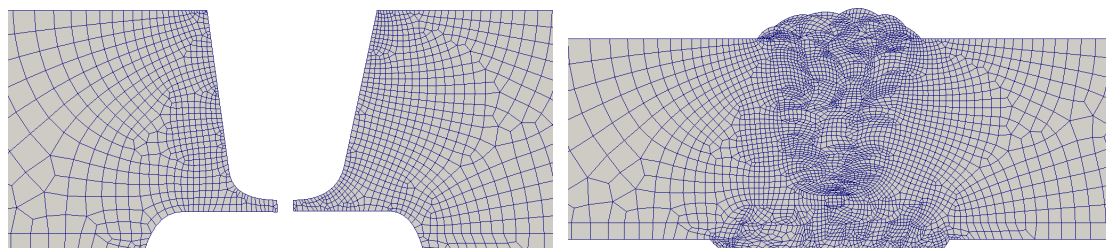
3 DETAILS OF THE NUMERICAL MODEL

The welding problem is numerically solved by making use of a staggered thermo-mechanical scheme, where in each time step, the thermal problem is solved first, and the mechanical problem solved next by taking as thermal state the previously computed temperature field. The

thermal problem is considered to be decoupled from the mechanical problem, because the energy variation generated by mechanical deformations is negligible when compared to the heat input to the medium (given by the welding torch).

No microstructural changes were taken into account. The contribution of solid-liquid transformations is computed as part of the thermal problem by making use of the linear triangular element presented by Fachinotti et al. (1999). It was observed by Mullins and Gunnars (2009) that when computing weld residual stresses in pipe welds, an isotropic hardening model better approximates experimental measurements than a kinematic or mixed hardening model. Following this observation, the mechanical behaviour of the material is described by an isotropic elasto-plastic hardening model. Quadrilateral Q1/P0 elements (Hughes, 2000) are used to solve the mechanical problem. Material deposition is handled by making use of the *inactive* element approach where, additionally, the concept of stress free configurations is taken into account (Anca et al., 2011a,b).

As depicted by Figure 4a the domain of the problem was discretised using 4722 quadrilaterals and 4885 nodes. The welding plan specified by Figure 3a was taken into account, and accordingly meshed as shown in Figure 4b. For the thermal problem, the triangular elements were generated from the quadrilateral mesh by dividing each of them into two triangles by the biggest angle criterion. A mesh of line segments defining the skin elements for the thermal Robin boundary condition was built and considered in the computations. This task requires some careful work, as skin elements associated to weld beads that are being deposited must be activated and subsequently deactivated as new weld beads are deposited. Figure 5 shows the different skin elements used as weld bead boundaries, and the order in which each weld bead is deposited, information that is specified by the numbers inside each weld bead.



(a) Detail of the mesh without weld beads deposited. (b) Detail of the mesh with all the weld beads deposited.

Figure 4: Details of the domain discretisation.

In this two dimensional axisymmetric analysis, a new layer of material or weld bead is deposited each time the weld torch crosses the section under analysis. Then, the material deposition and the heat input to the medium can be modelled by means of a simplified version of the Goldak heat source (Goldak et al., 1984) as similarly done in (Fachinotti et al., 2010, 2012). In this heat source model, it is supposed that the total heat power is uniformly distributed across the area Ω_L of the section of the last added layer of material. Then, heat input to the medium is given by the expression

$$Q_s(t) = \frac{\sqrt{3}Q}{\sqrt{\pi}\Omega_L} \begin{cases} \frac{f_f}{c_f} \exp\left(-3\frac{\theta(t)^2}{c_f^2}\right) & \text{if } \theta(t) \leq 0 \\ \frac{f_r}{c_r} \exp\left(-3\frac{\theta(t)^2}{c_r^2}\right) & \text{if } \theta(t) > 0 \end{cases} \quad (1)$$

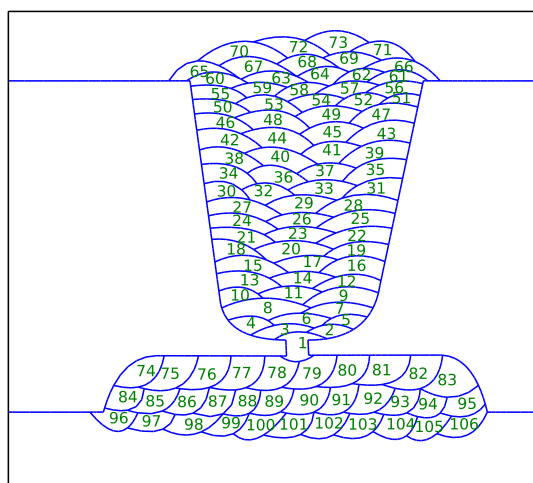


Figure 5: Skin elements used as part of the Robin boundary condition (take into account that these skin elements have associated activation and deactivation times). The numbers are used to denote the order in which weld beads are deposited, serving as definition of the weld plan.

where c_f and c_r are the length parameters associated with the axis of the front and rear semi-ellipsoids, f_f and f_r are the portions of heat distributed in the front and rear semi-ellipsoids, and Q is the total heat input. The function $\theta(t)$ gives the variation of position of the heat source in the circumferential direction. For the current application problem the heat source parameters were taken as $c_f = 5 \times 10^{-3}\text{m}$, $c_r = 4c_f$, $f_f = 2c_f/(c_f + c_r)$ and $f_r = 2 - f_f$. The tangential velocity of the heat source and the heat source parameter Q can be observed in Figures 6a and 6b.

The time increment Δt used in the time discretisation must be small enough in order to ensure that the heat source is well integrated. In order to correctly capture the behaviour of the heat source, it must traverse the section under analysis in 10 to 20 time steps (Fachinotti et al., 2012; Goldak et al., 1986). In other words, when the heat source is crossing the analysed section the time increment should be of the order

$$\Delta t = O\left(\frac{c_f + c_r}{nv}\right), \quad (2)$$

where n takes a value in the interval $n \in [10, 20]$ and v denotes the tangential velocity of the heat source. Once the heat source has crossed the section of analysis, the time increment can be increased. In this work the parameter n was taken equal to 10 and the time increment was linearly increased up to a maximum of 100s.

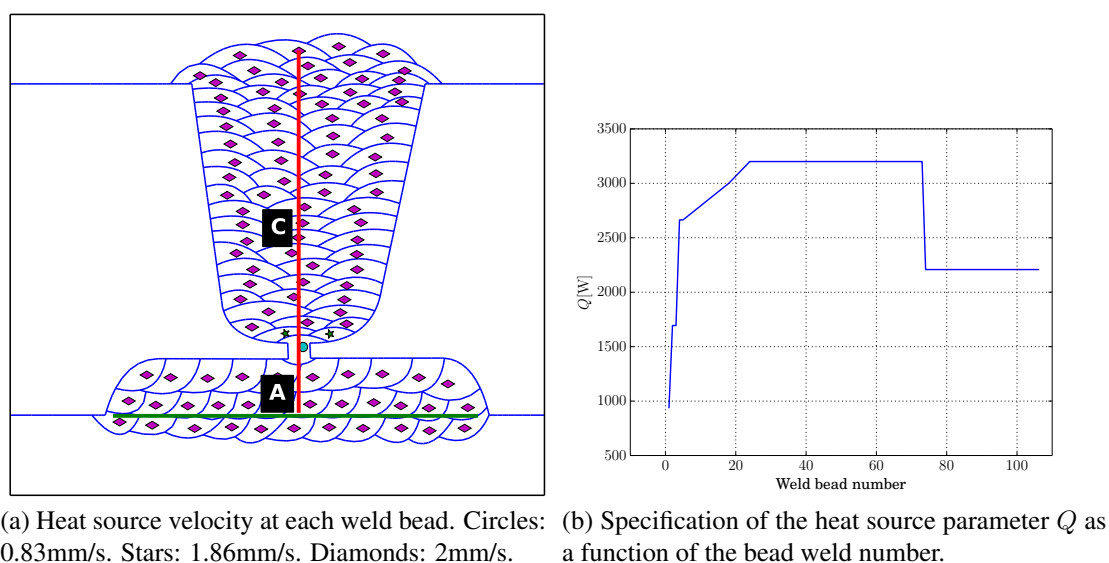


Figure 6: Details of the heat source parameters.

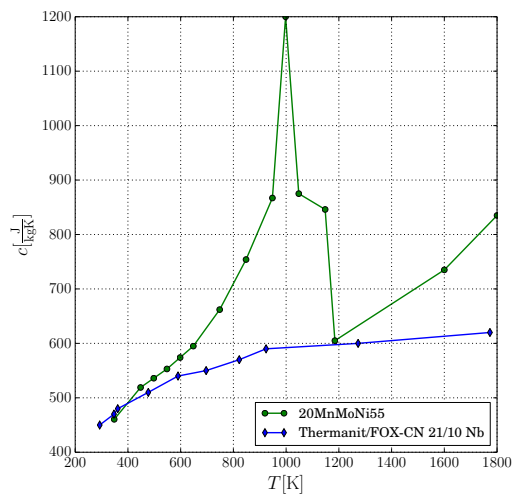
4 MATERIAL PROPERTIES

As previously observed in Figure 3b, the material of the nozzle and the pipe is the alloy 20MnMoNi55, the weld metal material is Tenacito 65R, the cladding material is FOX-CN 21/10 Nb and the back weld metal is Thermanit 25/14E. In the case of the materials 20MnMoNi55 and Tenacito 65R, it is supposed that both share the same thermal and mechanical properties except for the curves σ - α describing the plastic response of the material.

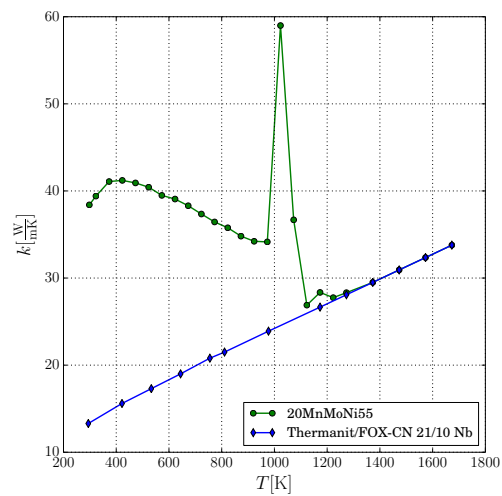
The materials designations 20MnMoNi55 (1.6310) and Tenacito 65R are similar to the US A508 material, the designation Thermanit 25/14E (1.4332) is similar to the steel 309L, and the material FOX-CN 21/10 Nb is similar to the steel 347. In what follows the thermal and mechanical properties of these materials are specified. In Table 1 the reference temperature T_{ref} , and the material parameters given by the zero strength temperature T_{zst} , the mass density ρ (taken as constant), the melting temperature T_m and the latent heat \mathcal{L} can be observed for each of the considered materials. The mass density for the materials 20MnMoNi55 and Thermanit 25/14E were estimated from the Material Property Database (mat, 2014). The material parameters ρ , T_m and \mathcal{L} were taken from (Sun and Moio, 1994). The material parameters T_m and \mathcal{L} for the other materials were estimated from data available at the website of Code Aster (www.code-aster.org). The parameter T_{zst} was taken as 98% of the melting temperature T_m . The other material properties are given in Figures 7a, 7b, 8b, 9a and 9b. The heat convection coefficient, specified in Figure 8a, was supposed to be equal to the one presented in (Anca et al., 2011a). The exponential law proposed by Voce (Voce, 1955) is adopted for describing hardening. Accordingly, the curves σ - α are given in Figures 10a, 10b, 11a and 11b were built by fitting the experimental curves. This fitting was accomplished using the function `curve_fit` of the python package `scipy.optimize` (Jones et al., 2001-).

Table 1: Some of the material parameters

Material	T_{zst}	T_{ref}	ρ	T_m	\mathcal{L}
20MnMoNi55	1715K	423K	$7870 \frac{\text{kg}}{\text{m}^3}$	1750K	$273190 \frac{\text{J}}{\text{kg}}$
FOX-CN 21/10	1639.5K	423K	$7750 \frac{\text{kg}}{\text{m}^3}$	1673K	$271960 \frac{\text{J}}{\text{kg}}$
Thermanit 25/14E	1592.5K	423K	$7980 \frac{\text{kg}}{\text{m}^3}$	1625K	$276940 \frac{\text{J}}{\text{kg}}$

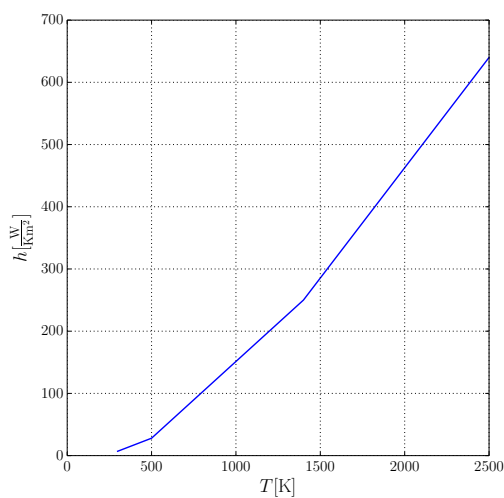


(a) Temperature dependent heat capacity.

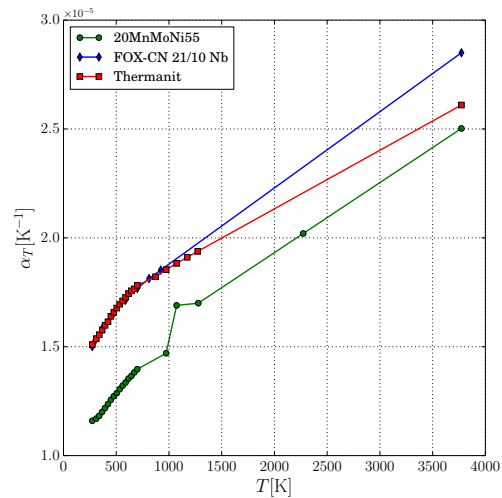


(b) Temperature dependent heat conductivity.

Figure 7: Thermal properties specification: heat capacity and heat conductivity.

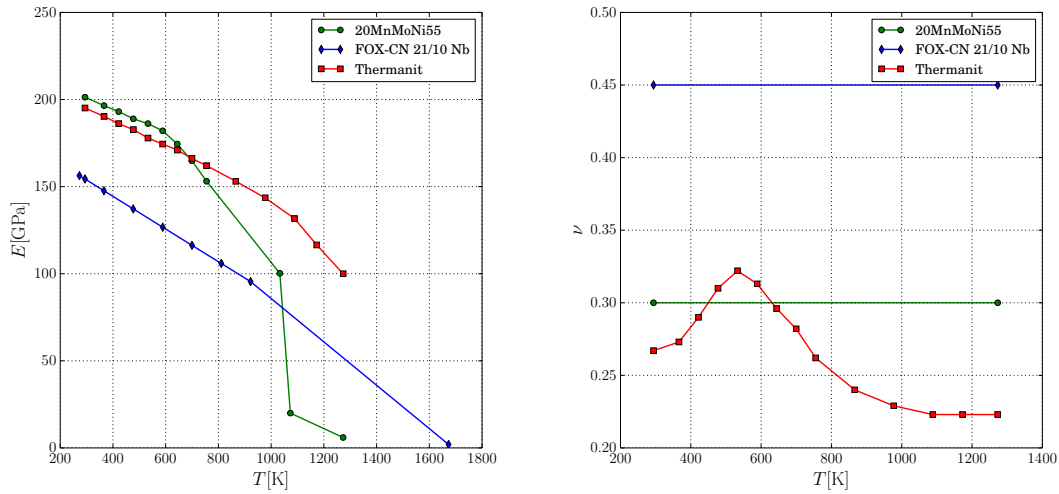


(a) Temperature dependent heat convection coefficient.



(b) Temperature dependent thermal expansion coefficient.

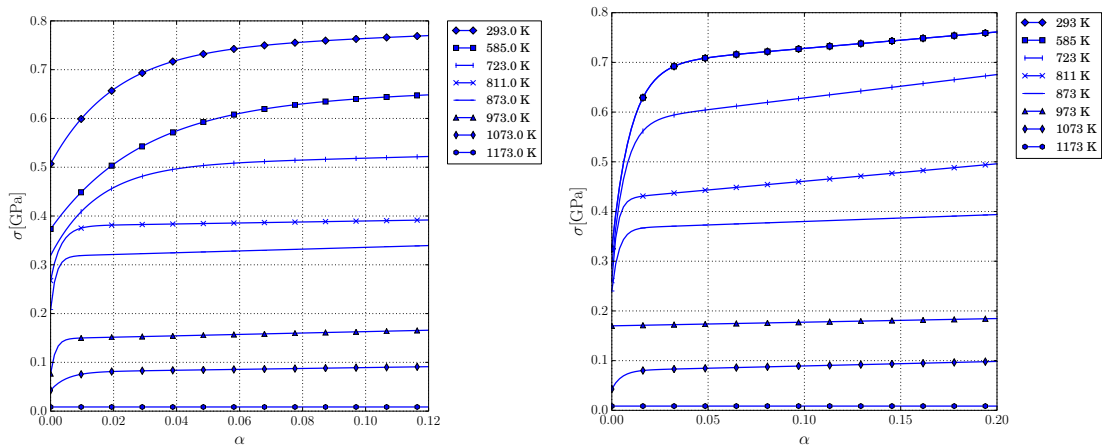
Figure 8: Heat convection coefficient and thermal expansion coefficient specification.



(a) Temperature dependent Young's modulus.

(b) Temperature dependent Poisson ratio.

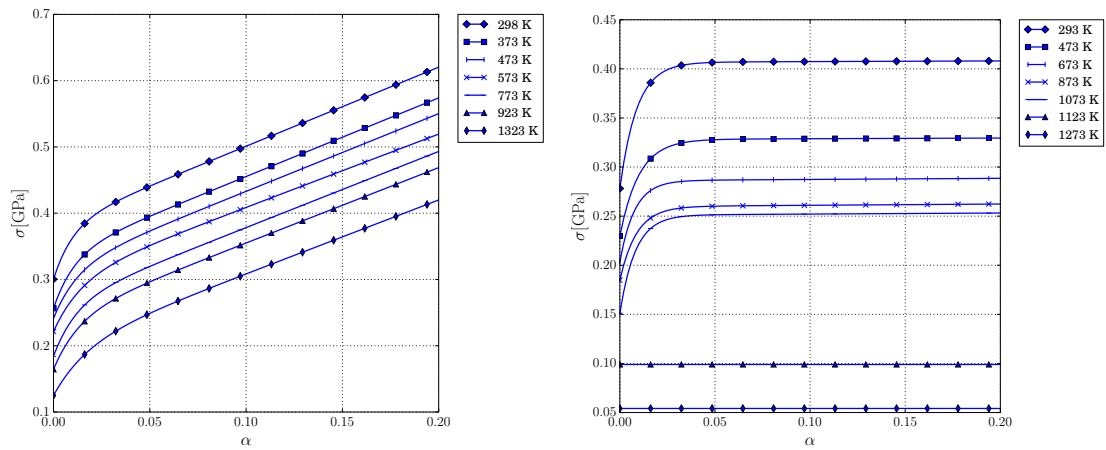
Figure 9: Mechanical properties specification: Young's modulus and Poisson ratio.



(a) Temperature dependent σ/α curves for the 20MnMoNi55 alloy.

(b) Temperature dependent σ/α curves for the weld metal.

Figure 10: Mechanical properties specification: σ/α curves for the materials 20MnMoNi55 and Tenacito 65R.



(a) Temperature dependent σ/α curves for the FOX-CN 21/10 Nb alloy. (b) Temperature dependent σ/α curves for the Thermanit alloy.

Figure 11: Mechanical properties specification: σ/α curves for the materials FOX-CN 21/10 Nb and Thermanit 25/14E.

5 RESULTS

The simulation was run up to attaining a maximum temperature of 302K. Approximately 12100 time steps were computed, taking an approximate computation time of $5887.4\text{s} = 1\text{h } 38\text{min}$ in a machine with the following specifications using four threads:

- Processor: Intel(R) Core(TM) i7 CPU 930 @ 2.80GHz.
- Number of physical cores: 4 cores; hyper-threading deactivated.
- Cache L1, L2, L3: 32KB, 256 KB, 8MB.
- Memory: 6GB.
- Operating system: `Linux 2.6.34.10 #1 SMP x86_64 GNU/Linux`.

The exportation of data to ParaView, a post-processing software (Henderson, 2007), took approximately $1025.9\text{s} = 17\text{min}$.

In Figures 12, 13 and 14 temperature profiles at different time instants of the welding process are shown. From these results it can be observed that the predicted temperature field is of good quality from the numerical point of view, and the heat source contribution is uniformly distributed as expected. In Figure 15 the amount of plastic distortion characterised by means of the equivalent plastic deformation α is shown. In the subsequent figures, specifically Figures 16, 17, 18 and 19, the components of the stress tensor can be observed, which specify the WRS at the end of the welding process.

In order to determine the influence of the solid-liquid phase change in the computed residual stresses, a simulation where no phase change is taken into account was performed. Then, the residual stress distribution along lines **A** and **B** depicted in Figure 6a was studied. The axial and hoop stresses along line **C** can be observed in Figures 20a and 20b, whereas these stresses along line **A** are shown in Figures 21a and 21b. A first conclusion is that solid-liquid phase change does not contribute in a considerable manner to the final residual stresses. This is an interesting finding that allows to simplify the thermal problem considerably, thus reducing the computation time. For example, in two dimensional problems it is no longer needed the use of triangular elements, making possible to use the cheaper quadrangular elements. The same is true for three dimensional problems where thermal tetrahedral elements can be replaced by thermal hexahedral elements. Take into account that in three dimensional problems when using tetrahedral elements the element count is six times larger than the number of required hexahedral elements. To understand why it is necessary to use triangles and tetrahedra when solving thermal problems where solid-liquid phase change is considered, it should be noted (Cosimo et al., 2012) that in order to predict the position of the phase change boundary for a given set of nodal temperatures, the field should be interpolated linearly otherwise this estimation is not possible or, at least, much more complicated (Storti et al., 1987). Another evident advantage of not considering the solid-liquid phase change is the increase in robustness.

In Figure 22 the magnitude of the displacement field and the deformed configuration are shown. At a first glance it seems that the results are of good quality, but when observing in more detail (Figures 23a and 23b) it is found that some elements are highly distorted. This is because the mesh of the whole welding plan is built at the beginning of the process without taking into account the, unknown, distortion suffered by the elements comprising the weld beads as the welding plan advances. Despite the distortion of these elements, the residual stresses are well predicted thanks to the use of stress free configurations. In other more specific problems

(Anca et al., 2011a) it is noted that this distortion is not so high, leading to the observation that this issue is more likely to arise in complex geometries and in situations where the extension of the welding plan increases, or, equivalently, where the number of weld beads is high. There are existing techniques aimed at solving this artificial distortion problem, as the one presented by Lindgren and Hedblom (2001) but whose complexity does not contribute to its applicability. In order to solve this issue more research is needed, and it is left as future work.

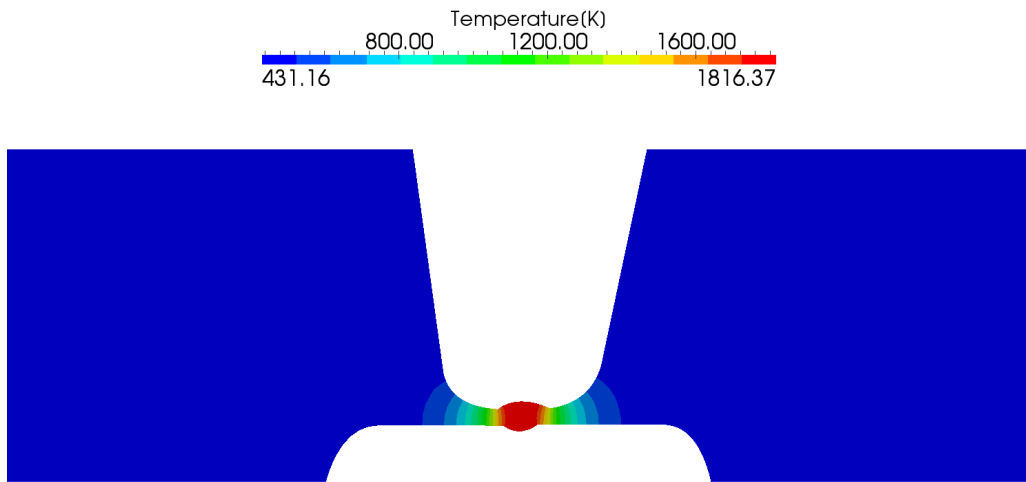


Figure 12: Temperature profile at the beginning of the process.

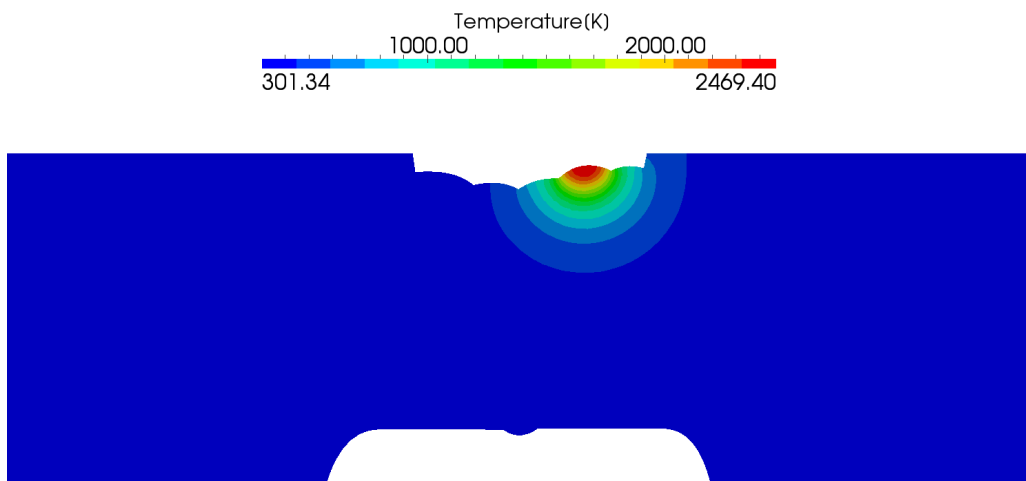


Figure 13: Temperature profile at the middle of the process.

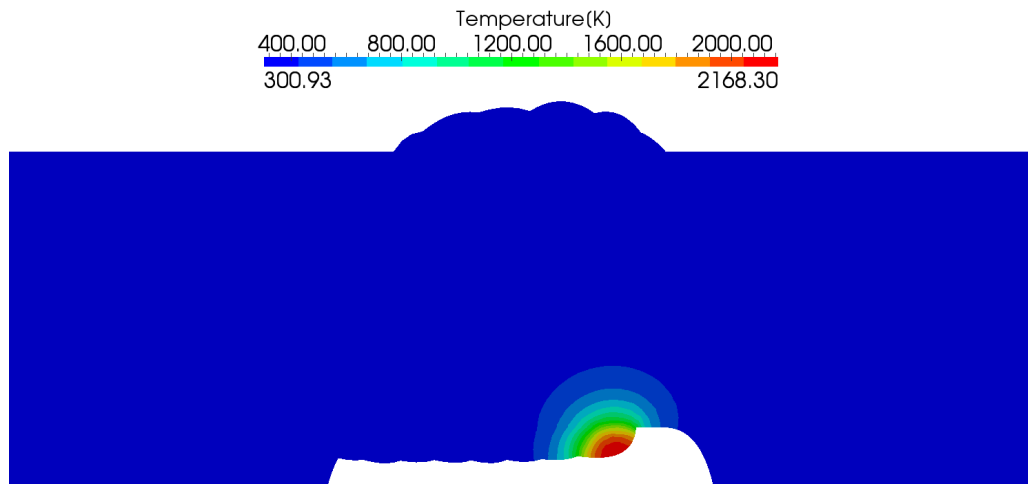


Figure 14: Temperature profile when depositing a weld bead at the back weld.

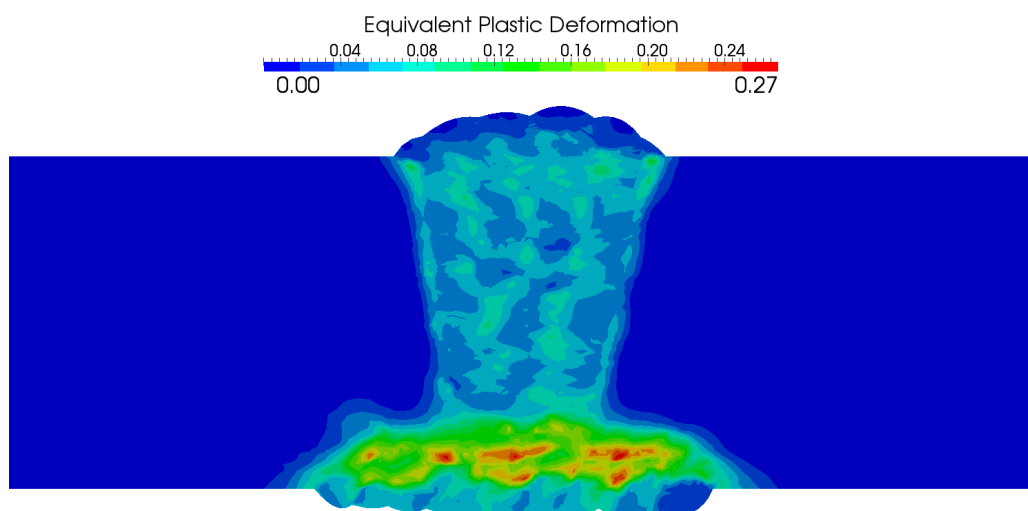


Figure 15: Resultant equivalent plastic deformation.

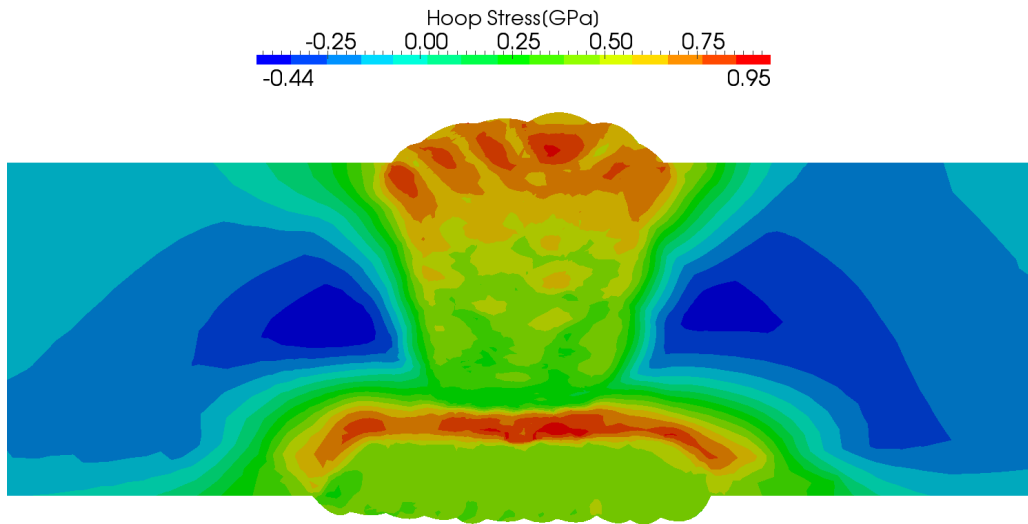


Figure 16: Residual stresses: Hoop stress.

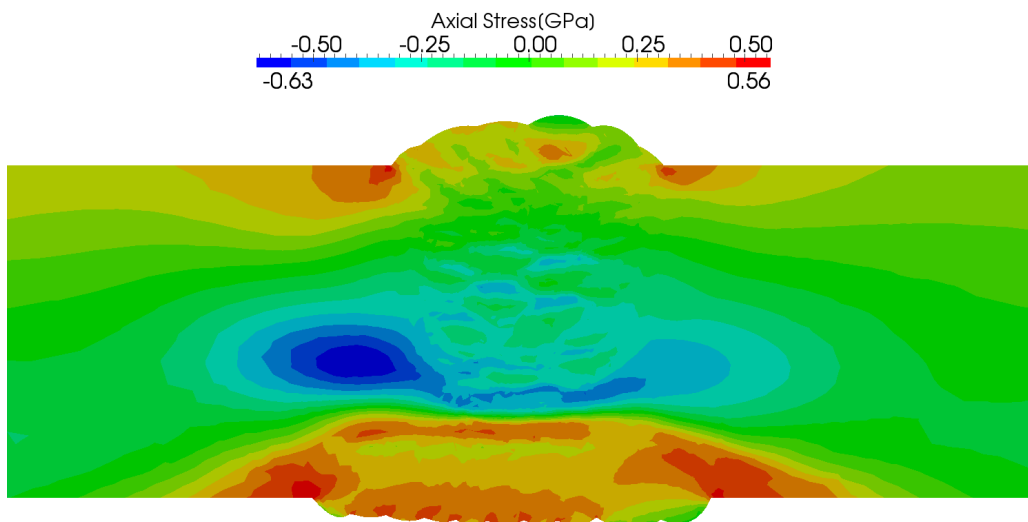


Figure 17: Residual stresses: Axial stress.

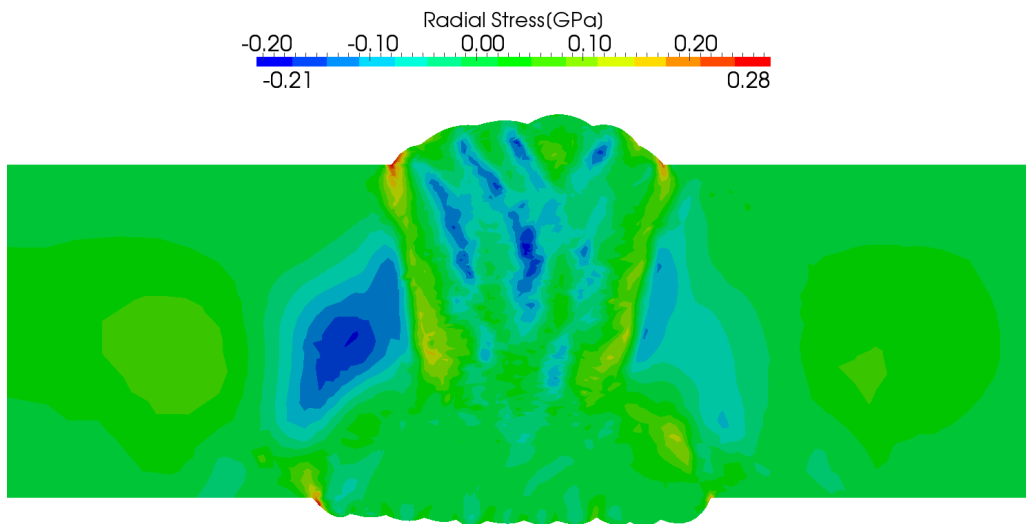


Figure 18: Residual stresses: Radial stress.

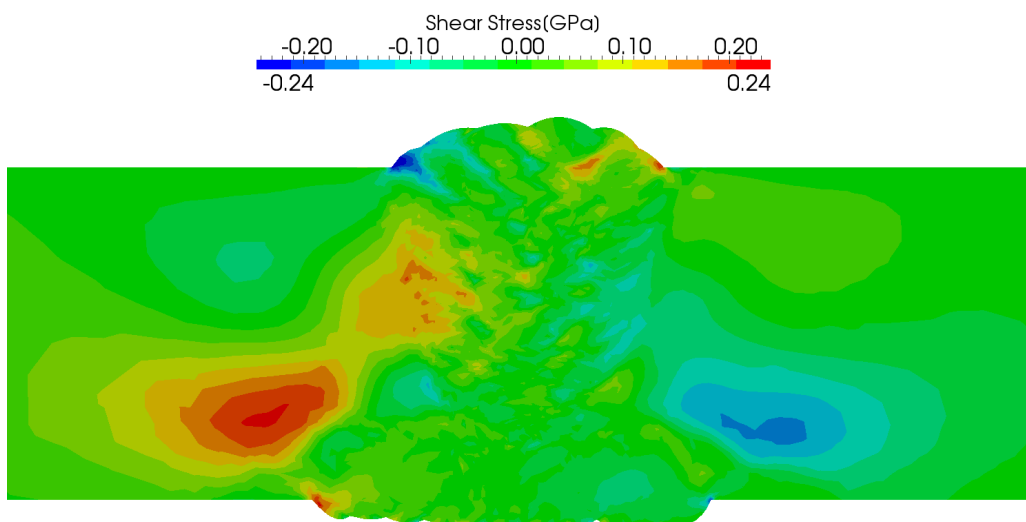
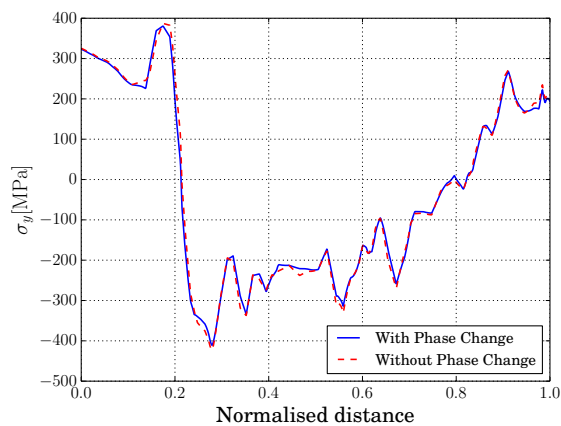
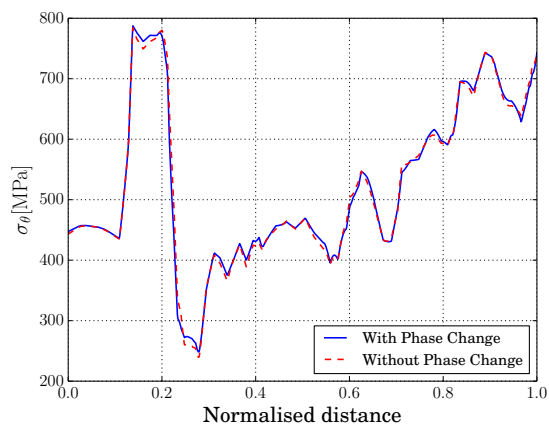


Figure 19: Residual stresses: Shear stress.

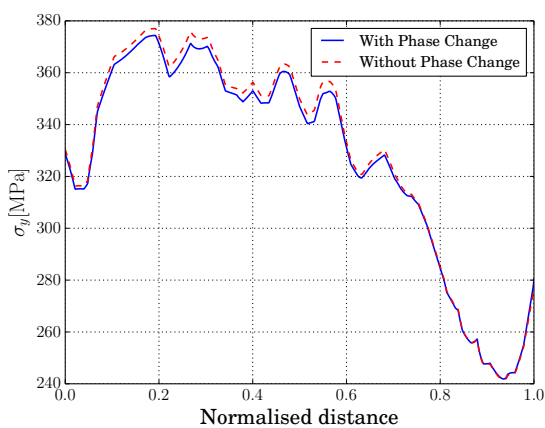


(a) Axial stress along line C.

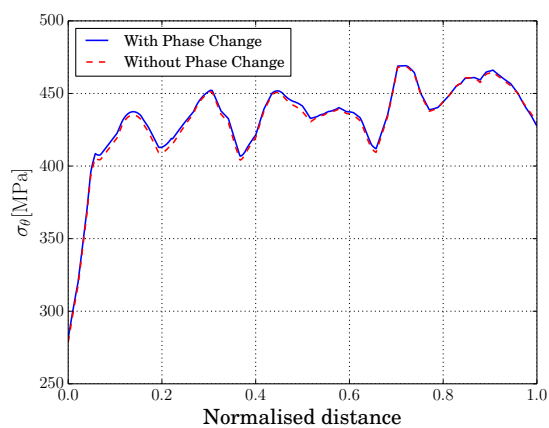


(b) Hoop stress along line C.

Figure 20: Residual stress components along the line C. Comparison of results obtained computing the contribution of solid-liquid latent heat and without it.



(a) Axial stress along line A.



(b) Hoop stress along line A.

Figure 21: Residual stress components along the line A. Comparison of results obtained computing the contribution of solid-liquid latent heat and without it.

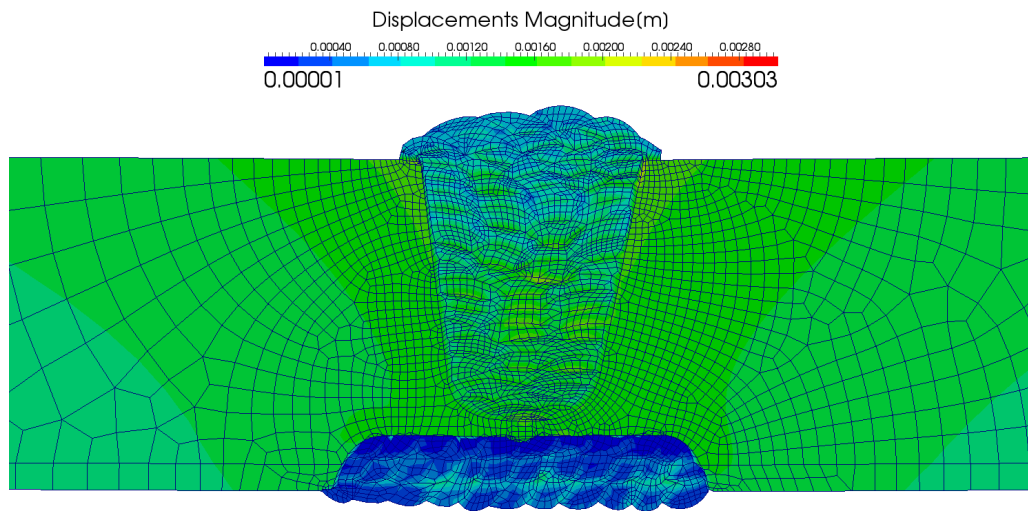


Figure 22: Displacement field and deformed configuration.

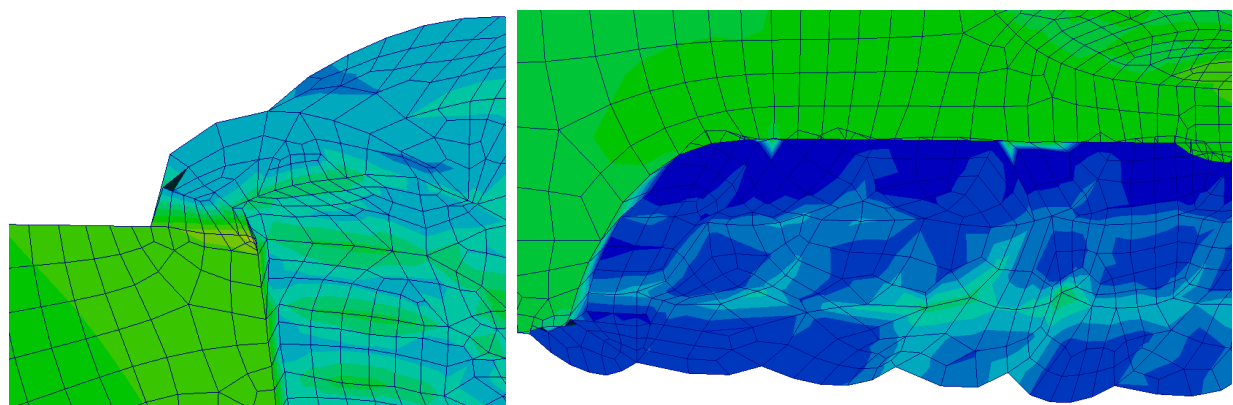


Figure 23: Details: displacement field and deformed configuration.

6 CONCLUSIONS

In this work, the simulation of the welding process of a nozzle weld that connects the RPV and the cold leg of a nuclear reactor facility was addressed. This problem was solved using a two dimensional axisymmetric model in order to reduce the computational complexity, approximation that is valid if the section under analysis is far enough from the starting and ending points of the weld. Following the remark of Mullins and Gunnars (2009), an isotropic elasto-plastic hardening model was used. Additionally, the hypothesis of small deformations was adopted. In the case of the thermal problem, two kinds of models were taken into account. On one of the models the contribution of the latent heat associated to the solid-liquid phase change was considered, and in the other this contribution was neglected. When comparing the obtained residual stresses it is evident that the latent heat of the solid-liquid phase change does not contribute significantly, leading to the conclusion that it would be advantageous not to compute solid-liquid phase change effects in order to gain in terms of computational efficiency and robustness.

Another finding was that due to the complexity of the geometry and the welding plan (the large number of weld beads), some elements suffered from high artificial distortion. Despite this situation, the computed residual stresses are well computed thanks to the use of stress free configurations. In future works, the investigation of new techniques dealing with this artificial distortion will be addressed. Additionally, the modelling of the PWHT will be considered.

REFERENCES

- Material property database. <http://www.jahm.com>, 2014.
- Anca A., Cardona A., Risso J., and Fachinotti V. Finite element modeling of welding processes. *Applied Mathematical Modelling*, 35(2):688–707, 2011a.
- Anca A., Fachinotti V., Escobar-Palafox G., and Cardona A. Computational modelling of shaped metal deposition. *International Journal for Numerical Methods in Engineering*, 85(1):84–106, 2011b.
- Cosimo A., Fachinotti V., and Cardona A. An enrichment scheme for solidification problems. *Computational Mechanics*, pages 1–19, 2012. Cited By (since 1996) 0; Article in Press.
- Fachinotti V., Cardona A., Cosimo A., Baufeld B., and Van der Biest O. Evolution of temperature during shaped metal deposition: Finite element predictions vs. observations. *Mecánica Computacional*, 19:4915–4926, 2010.
- Fachinotti V.D., Cardona A., Baufeld B., and der Biest O.V. Finite-element modelling of heat transfer in shaped metal deposition and experimental validation. *Acta Materialia*, 60(19):6621 – 6630, 2012. ISSN 1359-6454.
- Fachinotti V.D., Cardona A., and Huespe A.E. A fast convergent and accurate temperature model for phase-change heat conduction. *International Journal for Numerical Methods in Engineering*, 44(12):1863–1884, 1999. ISSN 1097-0207.
- Goldak J., Bibby M., Moore J., House R., and Patel B. Computer modeling of heat flow in welds. *Metallurgical Transactions B*, 17(3):587–600, 1986. ISSN 0360-2141. doi:10.1007/BF02670226.
- Goldak J., Chakravarti A., and Bibby M. A new finite element model for welding heat sources. *Metallurgical and Materials Transactions B*, 15:299–305, 1984. ISSN 1073-5615.
- Henderson A. Paraview guide, a parallel visualization application. Kitware Inc., 2007.
- Hughes T. *The finite element method: linear static and dynamic finite element analysis*. Dover Publications, 2000.
- Jones E., Oliphant T., Peterson P., et al. SciPy: Open source scientific tools for Python. 2001–.

- Lindgren L.E. and Hedblom E. Modelling of addition of filler material in large deformation analysis of multipass welding. *Communications in Numerical Methods in Engineering*, 17(9):647–657, 2001. ISSN 1099-0887. doi:10.1002/cnm.414.
- Mullins J. and Gunnars J. Influence of hardening model on weld residual stress distribution. Technical Report 2009:16, Inspecta Technology AB, Stockholm, Sweden, 2009.
- Storti M., Crivelli L.A., and Idelsohn S.R. Making curved interfaces straight in phase-change problems. *International Journal for Numerical Methods in Engineering*, 24(2):375–392, 1987. ISSN 1097-0207.
- Sun Z. and Moio T. Melting ratio in laser welding of dissimilar metals. *Journal of Materials Science Letters*, 13(13):980–982, 1994. ISSN 0261-8028. doi:10.1007/BF00701444.
- Voce E. A practical strain-hardening function. *Metallurgica*, 51:219–226, 1955.